Articles

Ultraviolet Resonance Raman Examination of Horse Apomyoglobin Acid Unfolding Intermediates†

Zhenhuan Chi and Sanford A. Asher*

Department of Chemistry, Chevron Science Center, University of Pittsburgh, Pittsburgh, Pennsylvania 15260

Received November 6, 1998; Revised Manuscript Received April 21, 1999

ABSTRACT: We have used UV resonance Raman spectroscopy to study the acid-induced denaturation of horse apomyoglobin (apoMb) between pH 7.0 and 1.8. The 206.5 nm excited Raman spectra are dominated by amide vibrations, which are used to quantitatively determine the apoMb secondary structure. The 229 nm excited Raman spectra are dominated by the Tyr and Trp Raman bands, which are analyzed to examine changes of Tyr and Trp environments and solvent exposures. We observe two partially unfolded apoMb intermediates at pH 4 and pH 2, while we observe only one partially unfolded holoMb intermediate at 2, in which the G and H helices are mainly intact, while the rest of protein is unfolded. This partially unfolded holoMb intermediate at pH 2 is essentially identical to the pH 2 apoMb intermediate. The partially unfolded pH 4 apoMb intermediate is composed of the three folded A, G, and H helices and contains 38% helical structure. The changes in the Trp Raman cross sections during the acid-induced denaturation indicates that Trp 7 is likely to be fully exposed in the apoMb pH 4 intermediate and that the A helix melts with a p$K_a \sim 3.5$.

Numerous laboratories around the world are presently investigating the theoretical and experimental aspects of "the protein folding problem" (*1*−*14*). For most proteins the essential nature of the problem is that, although it is clear that their primary sequence contains the complete recipe for protein folding, there is still little understanding of the molecular structural dynamics that lead from the unfolded to the native protein structure. The challenge in identifying the mechanistic steps involved in folding, results from the fact that protein folding is generally cooperative, which prevents the buildup of protein folding intermediates. This hinders experimental investigations since only the unfolded and fully folded states are populated.

A useful approach to examining the protein folding mechanism is to study in detail the few known proteins that display stable intermediates; the idea is to partition the protein folding problem into simpler steps that can be more easily characterized. This is why myoglobins (Mb) have been so intensely utilized as a model system in protein folding investigations. Sperm whale Mb, the first protein whose three-dimensional structure was characterized (*15*), forms a partially unfolded apoMb intermediate upon removal of the heme (*6, 16*). ApoMb undergoes further unfolding under denaturation conditions such as low pH or in the presence of urea, for example. Numerous studies have characterized these intermediate forms (*6, 7, 17*−*20*). More importantly, these apoMb equilibrium intermediates appear to be highly similar to early kinetic intermediates in the apoMb folding process (*6, 7*). Thus, the examination of apoMb equilibrium intermediates may give information on the actual protein structural intermediates involved in the protein folding pathway.

We have been developing UV resonance Raman spectroscopy for use in static protein structural investigations (*14, 21*−*28*) and have more recently used this approach for nanosecond protein folding studies (*29*). We have developed powerful methodologies to determine secondary structure in low concentration protein solutions under both static and dynamic conditions. In addition, we have developed methods to examine the environment of Tyr and Trp residues and have developed a quantitative methodology to determine the Tyr and Trp aromatic ring exposure to the aqueous solution (*14, 27, 30*).

In the present study, we examine the acid denaturation of horse apoMb by monitoring the 206 nm UV Raman spectral amide vibrations to determine the pH dependence of its secondary structure, and we have utilized the 229 nm UV Raman spectral Trp and Tyr vibrations to probe the pH dependence of the Trp and Tyr solvent exposure as the apoMb α-helices melt. We also compare the acid denaturation of apoMb to that of holoMb to probe the role of the heme in the holoMb structural stability.

EXPERIMENTAL PROCEDURES

Horse heart metmyoglobin (holoMb) was purchased from Sigma (St. Louis, MO) and used as received. ApoMb was prepared from holoMb by the method used by Teale (*16*).

† This work received support from NIH Grant R01GM30741-16.

* To whom correspondence should be addressed: Phone (412) 624-8570; Fax (412) 624-0588; E-mail asher+@pitt.edu.

10.1021/bi982654e CCC: $18.00
Published on Web 06/11/1999

The apoMb solution was filtered and then purified by Sephedex-25 gel chromatography. Absorption spectral measurements indicate an apoMb heme contamination of <1%. ApoMb concentrations were determined by using a molecular extinction coefficient at 280 nm of 14 620 M^{-1} cm^{-1} (*31, 32*). We utilized 18 μM holo- and apoMb solutions for the 206.5 nm Raman measurements and 80 μM solutions for the 229 nm Raman measurements. The sample solution pH values were adjusted by adding small amounts of concentrated HCl and KOH solutions with rapid stirring. These unbuffered solutions contained only the counterions added during the titration to achieve the solution pH values. For example, the pH 2 holo- and apoMb samples contained ~15 mM Cl^-. We saw no evidence of protein precipitation during the titrations and Raman spectral measurements. Also we found the pH = 2 titration of both holo- and apoMb to be completely reversible over the 15-min time period of our low-pH Raman spectral measurements.

The Raman cross section of the 932-cm^{-1} band of sodium perchlorate, previously determined by Dudik et al. (*33*), was used to calculate the Raman cross sections of Trp and Tyr. The ~500-cm^{-1} water librational Raman bands (*34*) were used as an internal intensity standard to determine the apoMb Raman cross sections. We separately determined the water librational band Raman cross sections by measuring the relative intensity of this band compared to that of the perchlorate 932-cm^{-1} band. The Raman cross sections were determined by peak height measurements.

UV Raman measurements were obtained by using instrumentation described in detail previously (*14, 35*). CW laser excitation was obtained from intracavity frequency-doubled Kr ion (206.5 nm, 1.5 mW) and Ar ion (229 nm, 7 mW) lasers, respectively (*36, 37*). The higher concentration 229 nm excitation experiments used a wire-guided jet sampling system similar to that of Cho et al. (*24*) to avoid photodegradation. For the 206.5 nm excitation experiments, the sample solutions were pumped through a 1.0 mm i.d. Supersil quartz capillary. An 1800 groove/mm grating was used in second order. We utilized spectral resolutions of 8.5 cm^{-1} for 229 nm excitation and 20 cm^{-1} for 206.5 nm excitation. The spectra were detected by using an ICCD (1024 × 256 pixels, Princeton Instruments, Princeton, NJ) with a total accumulation time of 20 min. Absorption spectra were measured by using a Perkin-Elmer Lambda-9 spectrometer.

RESULTS AND DISCUSSION

Absorption Spectral Changes. Figure 1 shows the pH dependence of the apoMb absorption spectra between pH 7.0 and 2.0, while the insets show the pH dependence of absorbance at 200 and 230 nm and expanded spectra between 222 and 240 nm. Below 210 nm the spectra are dominated by the $\pi-\pi^*$ electronic transitions of the protein backbone. The Tyr and Trp residues give rise to the shoulder between 210 and 230 nm (*14*). The apoMb absorption spectra are independent of pH between pH 7.0 and 5.3; however, pH decreases from pH 5.3 to 3.0 result in an increased 200−220 nm absorption and a decreased 230 nm absorption. The apoMb absorption spectra show few additional changes as the pH decreases from pH 3.0 to 1.8.

These spectral changes are qualitatively similar to those we observed previously for holoMb (*14*), which correlate

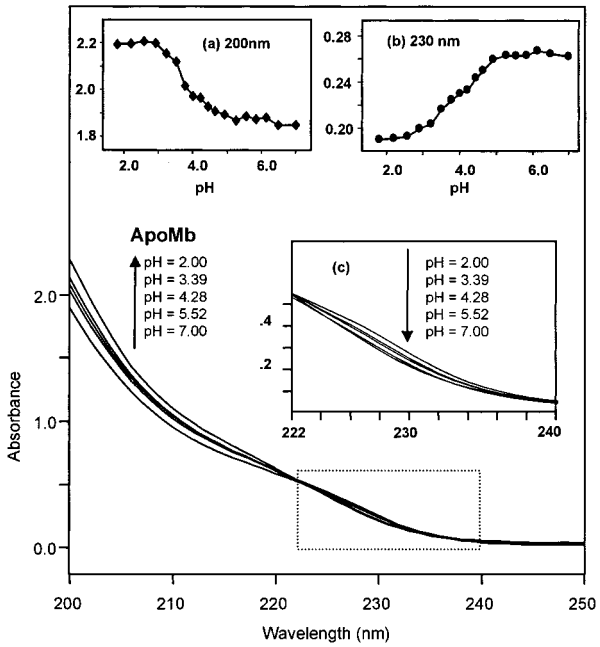

FIGURE 1: Horse apomyoglobin (5.0 μM) absorption spectra at various pH values. Inset (a) plots the pH dependence of the 200 nm apoMb absorbance. Inset (b) plots the pH dependence of the 230 nm apoMb absorbance. Inset (c) shows the absorption spectra between 222 and 240 nm. The spectra were measured in a 5-mm path length cell.

with the known unfolding of the apoMb α-helical structure (*6*, *7*, *17*−*20*, *27*, *38*); the absorption increase below ~210 nm results from hyperchroism of the peptide amide $\pi-\pi^*$ electronic transitions, due to decreased excitonic interactions in the unordered peptide conformations compared to those in the α-helical conformations (*14, 22, 27, 39*). The small ~230 nm apoMb absorption decrease appears qualitatively similar to that observed in the acid unfolding of holoMb; unfolding exposes the Trp side chains to water, which red-shifts their aromatic ring $\pi-\pi^*$ transition frequencies (*14, 30*).

In comparison to the pH dependence of the absorption spectra of holoMb, where changes only occur between pH 3.75 and 3.25 (*14*), the apoMb absorption spectra change continuously over the entire region between pH 5.5 and 3.0. These continuous apoMb absorption spectral changes indicate a more gradual acid unfolding of apoMb, compared to holoMb.

UV Raman Studies of Secondary Structure. Figure 2 shows the 206.5 nm excited resonance Raman spectra of apoMb at pH values between pH 7.00 and 1.78. These spectra are dominated by amide vibrations, since this excitation is resonant with the amide $\pi-\pi^*$ transitions (*27, 40*). The spectra show a strong enhancement of the amide I band (~1660 cm^{-1}), which is predominantly carbonyl stretching; a significant enhancement of the ring stretching vibrations of Tyr and Trp aromatic amino acid side chains (~1610 cm^{-1}) (*14, 30, 41*−*44*); a strong enhancement of the amide II band (~1555 cm^{-1}), which involves a large contribution of C−N stretching and N−H bending; a variable amide C_α−H bending vibration (1386 cm^{-1}); and a strong enhancement of the amide III vibration (1240−1300 cm^{-1}), whose composition is similar to that of amide II vibration, except that opposite phasing occurs between C−H stretching and N−H bending (*22, 25*−*27*).

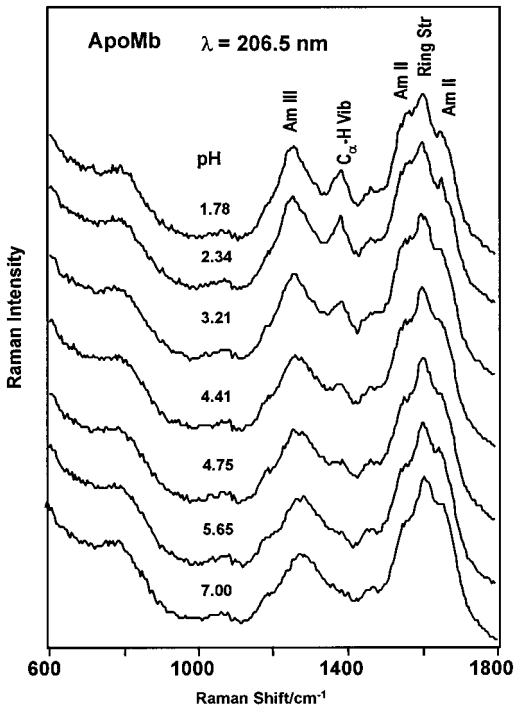

FIGURE 2: Raman spectra (206.5 nm excitation) of apoMb (18 μM) at various pH values. The spectra were detected by an ICCD detector, with a total accumulation time of 20 min. An 1800 grooves/mm grating was used in second order, giving a spectral resolution of ~20 cm^{-1}.

The apoMb amide Raman spectra are essentially identical between pH 7.0 and 5.6. The spectra show a strong amide I (~1655 cm^{-1}), a medium-intensity amide II band (~1555 cm^{-1}), a very weak amide C_α−H bending vibration (1386 cm^{-1}); and a broad amide III band (~1278 cm^{-1}), which indicates that most of the apoMb secondary structure is α-helical (*22, 27*).

As the pH decreases from 5.6 to 3.2, the 1386 cm^{-1} C_α−H bending band intensity increases, the amide III band frequency downshifts from 1278 to 1260 cm^{-1} and the amide I band intensity decreases slightly. These spectral changes indicate an unraveling of the apoMb α-helical structure (*27*). A further pH decrease from 3.2 to 1.8 causes little further Raman spectral change, which indicates little further alteration in the apoMb secondary structure.

We utilized the previously developed pure secondary structure Raman spectra (PSSRS) methodology (*27*) to quantitatively calculate the apoMb secondary structure composition at the various pH values. Prior to PSSRS modeling, we subtracted from the measured apoMb spectrum both the Raman spectra of water and the Tyr, Trp, and Phe aromatic side chain Raman bands, as previously described (*27*). In addition, we excluded the 1610- and the 1450-cm^{-1} regions from the PSSRS modeling. Figure 3 shows the measured apoMb spectra used for the modeling as well as the residuals between the measured and calculated spectra. The small residuals demonstrate the excellence of the modeling.

Table 1 tabulates our calculated apoMb secondary structure abundances at the different pH values, while Figure 4 displays the pH dependence of the α-helical content of both apoMb and holoMb. At neutral pH a lower α-helical content exists for apoMb (~62%) compared to holoMb (~80%). This

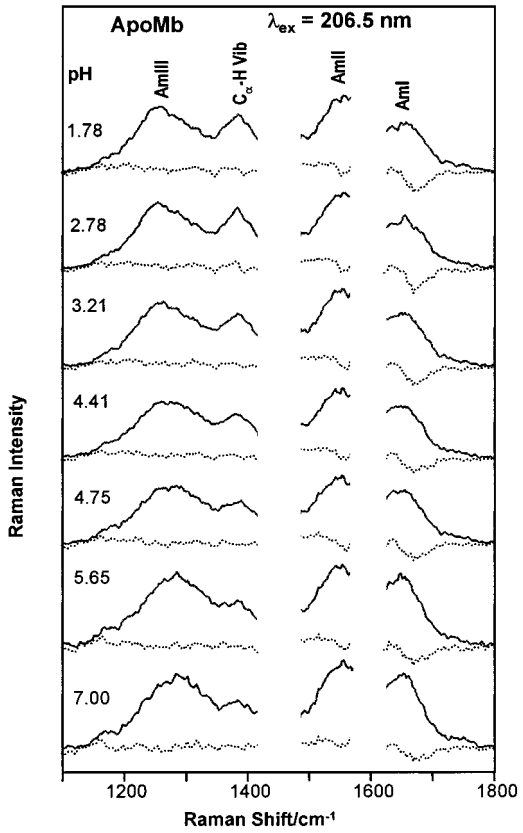

FIGURE 3: PSSRS modeling of the measured 206.5 nm excited Raman spectra (—) of apoMb (18 μM) at various pH values and the residuals (•••) (1100−1800 cm^{-1}). Before PSSRS modeling, we subtract from the measured protein spectrum both the Raman spectra of water and the Tyr, Trp, and Phe side chains, as previously described (*27*). In addition we exclude the ~1610- and 1450-cm^{-1} spectral regions.

Table 1: pH Dependence of Horse ApoMb Secondary Structure Composition

pH	α-helix (%)	β-sheet (%)	unordered (%)
7.00	61	0	39
6.02	62	0	38
5.65	62	0	38
5.32	60	1	38
5.05	57	4	39
4.75	50	4	46
4.41	44	9	47
4.14	39	8	53
3.82	37	20	43
3.52	34	13	53
3.21	27	17	56
2.78	21	14	65
2.34	19	0	81
1.78	19	0	81

~62% α-helical content of apoMb remains unchanged as the pH decreases to ~5.6, but decreases as the pH decreases from 5.6 to 3.0. Few further structural changes are observed for pH decreases below 3.0. The pH 4 intermediate observed contains ~38% helical structure, while the pH 2 state contains ~20% helix. A detailed discussion of the reliability of these secondary structure determinations is given in ref *27*. For example, this methodology gives a holoMb pH 7 α-helix content within 2% of that found by X-ray crystallography. Attempts to model the spectra with α-helix contents more than a few percent difference from those calculated gave poor residuals. Thus, we expect α-helix content

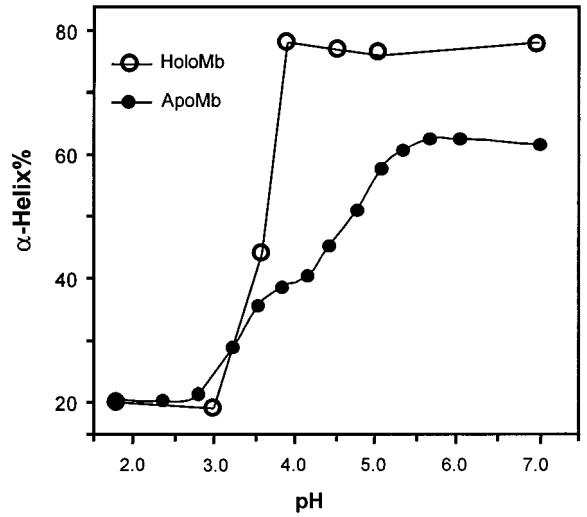

FIGURE 4: pH dependence of the calculated apoMb (●) and holoMb (○) α-helical composition calculated by using the PSSRS methodology.

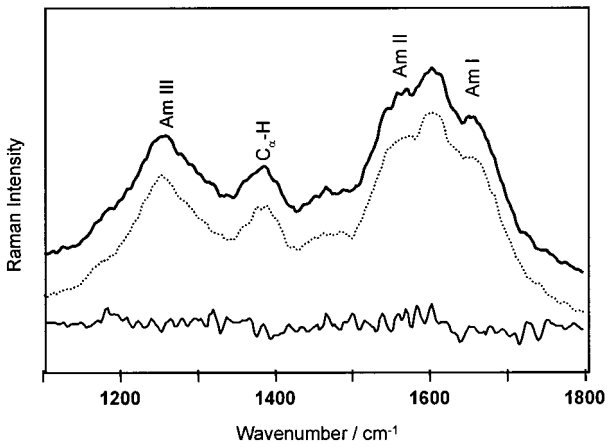

FIGURE 5: Raman spectra (206.5 nm excitation) of apoMb (—) and holoMb (•••) at pH 2.0 and the difference spectrum of apoMb minus holoMb (bottom). The concentrations of apoMb and holoMb are 18 μM.

accuracies of better than 3%, absolute.

The fact that the Figure 5 pH 2 Raman spectra of apoMb and holoMb are identical (their difference spectrum shows no recognizable features) indicates that apoMb and holoMb have essentially identical secondary structures at pH 2. We earlier assigned the holoMb pH 2 intermediate to a state where the entire protein is unraveled except for the sections of the G and H helices near the C-terminus (*14*). Thus, we can now assign the low-pH apoMb intermediate to an identical state, as is further confirmed by the UV Raman Tyr studies discussed below.

Goto et al. (*45, 46*) demonstrated that low-pH (<2) apoMb can form molten-globule-like states containing variable but significant α-helix content in the presence of anions such as Cl^-. The titrations of holo- and apoMb to low pH are unavoidably accompanied by an increased concentration of titrating counterions, which change the solution ionic strength. This could confound our understanding of the low-pH secondary structural transitions and could make the apoMb states dependent on the titrating anions. We cannot rule out that our observation of the existence of a 20% pH 2 α-helix content results from these salt-stabilized molten globule states

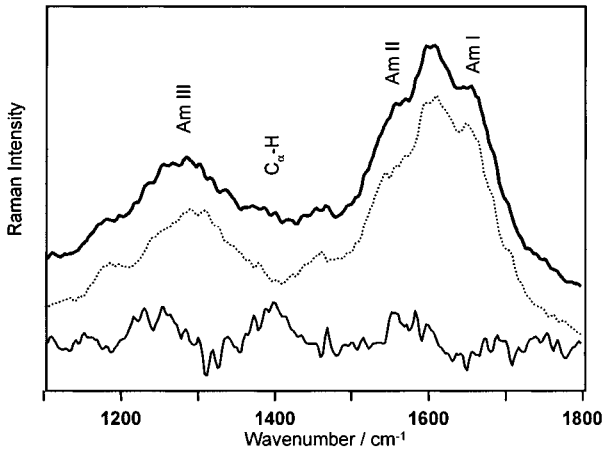

FIGURE 6: Raman spectra (206.5 nm excitation) of apoMb (—) and holoMb (•••) at pH 7.0 and the difference spectrum of holoMb minus apoMb (bottom). The concentrations of apoMb and holoMb are 18 μM.

(*45−47*). However, our ∼ 15 mM Cl^- concentrations would appear to be at the lowest possible edge for anion stabilization. Further, the pH independence of the holo- and apoMb α-helix content between pH 3 down to 1.5 (*14*) suggests that this is the low-pH maximally unfolded state.

The presence of the heme seems to stabilize the holoMb structure because apoMb begins unfolding at a higher pH than does holoMb; the apoMb α-helical content begins to decrease at pH < 5.65, while holoMb shows α-helix content decreases only for pH < 4. In fact, we see two stages of apoMb unfolding with apparent pK_a values of 4.8 and 3.5. Thus, we observe three different states of apoMb above pH 1.8, none of which are fully unfolded. In contrast, for holoMb we see only two states.

Figure 6 shows the Raman spectra of apoMb and holoMb at pH 7.0 and their Raman difference spectrum. The difference spectrum indicates an ∼18% α-helix content decrease in apoMb versus holoMb. We can interpret much of the horse Mb secondary structural changes observed here from the extensive previous investigations of sperm whale apoMb (*6, 7*). This is because these proteins have very similar primary sequences, and their high-resolution X-ray structures are almost identical (*48*). This allows us to assign the decreased α-helix content of apoMb versus holoMb mainly to melting of the F-helix, which in holoMb is spatially isolated from the remainder of the protein by the heme group (*17−19, 48−50*). Removal of the heme destabilizes the F helix, because of the loss of the His93 ligation to the heme iron as well as the loss of the numerous hydrophobic contacts between the F helix and the heme ring (*49, 50*). In addition, the NMR measurements of Eliezer and Wright (*49*) indicate melting of the nonhelical EF loop in apoMb. The remaining 8% decrease in α-helical content probably results from melting of the C and D helices, which in holoMb contains ∼7% α-helical structure. These are known to be the least stable helices in horse holoMb (*48*). Thus, we conclude that helices C, D, and F unravel upon removal of the heme, while helices A, B, E, G, and H remain intact in apoMb at neutral pH.

Further apoMb unfolding occurs as the pH decreases to 4; the pH 4 intermediate contains 38% α-helix content. The decreased α-helix composition at pH 4 appears to result from the melting of the B and E helices, in view of the previous

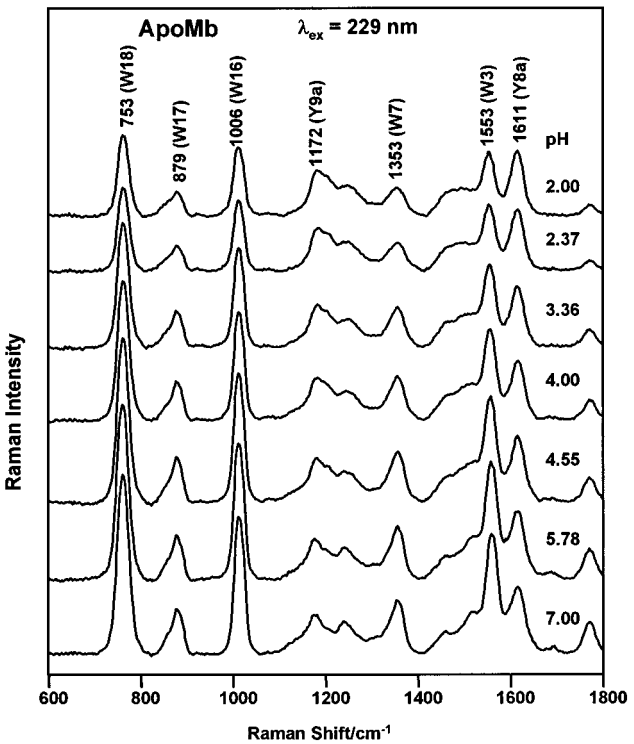

FIGURE 7: Raman spectra (229 nm excitation) of apoMb (90 μm) at various pH values. The spectra were detected by an ICCD detector, with a total accumulation time of 10 min. A 1800 grooves/mm grating was used in second order, giving a spectral resolution of ~8.5 cm^{-1}.

NMR and circular dichroism studies of sperm whale apoMb (*6, 7, 38, 51*), which show an intermediate unfolded apoMb state that contains a mainly intact domain involving the A, G, and H helices. It is likely that our unfolded pH 4 horse apoMb state has a similar domain since X-ray diffraction studies of holoMb indicate that these helices account for 40% of the holoMb helical structure (*48*).

UV Raman Studies of Trp and Tyr Environments. Important information on the location of acid-induced conformational changes can be obtained from the aromatic amino acid Raman spectra. Excitation at 229 nm within the strong Tyr and Trp $\pi-\pi^*$ transitions results in selective enhancement of Tyr and Trp bands, with negligible interference from either amide bands or those of any other amino acid side chain (*14, 30, 41−44*). Figure 7 shows the pH dependence of the 229 nm excited Raman spectra of apoMb. The 753-, 857-, 879-, 1012-, 1353-, and 1553-cm^{-1} bands derive from Trp, while the 1172- and 1207-cm^{-1} bands derive from Tyr. The 1611-cm^{-1} band derives mainly from the Tyr Y8a band, but a small contribution also occurs from the Trp W1 band.

As observed for holoMb, the Trp, but not the Tyr-cross sections decrease as the pH decreases (Figure 8). The lack of Tyr cross section changes, shown in Figure 8B, indicates the lack of structural alterations around Tyr 103 in the G helix and Tyr 146 in the H helix. This lack of change in the water exposure of these Tyr residues allows us to conclude that, as in holoMb, the G and H helix domains around the Tyr remain intact at pH 2 (*14, 30*).

In contrast, the sum of the Trp 7 and Trp 14 Raman intensities of the apoMb 1012-cm^{-1} Trp band decreases almost 2.5-fold as the pH decreases from 7.0 to 2.0. Our previous study of holoMb showed that the Trp Raman cross

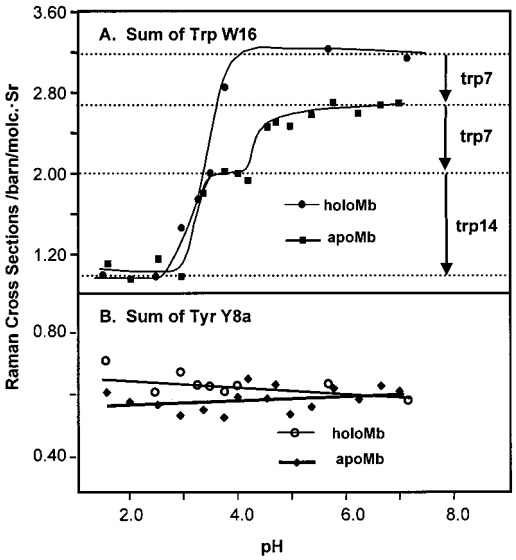

FIGURE 8: (A) pH dependence of the sum of the Trp 7 and Trp 14 229 nm excited apoMb (■) and holoMb (●) Trp W16 Raman band cross sections. The water band at ~500 cm^{-1} was used as an internal intensity standard to determine the Raman cross sections. (B) pH dependence of the 229-nm excited apoMb (◆) and holoMb (○) average Tyr Y8a Raman cross sections. The water band at ~500 cm^{-1} was used as an internal intensity standard to determine the Raman cross sections.

sections decrease due to exposure of the Trp rings to water during the A-helix acid unfolding (*14, 30*). For holoMb the acid unfolding is relatively simple with a single transition with a pK_a ~ 3.5 to form this pH 2 unfolded intermediate. At pH 2 the Trp rings appear to be completely exposed to water. In contrast, Figure 8A shows a complicated pH dependence for the apoMb Trp Raman cross sections, which is consistent with the Figure 4 α-helix melting behavior and also indicates two well-separated unfolding transitions. For apoMb the Trp Raman cross sections remain relatively constant as the pH decreases from 7.0 to 5.5 and then begin to gradually decrease until a precipitous drop at pH ~ 4.4. The Raman cross sections then remain invariant until a second precipitous drop at pH ~ 3.2. No additional Trp Raman cross section changes occur between pH 3.0 and 1.5.

We recently (*14, 30*) demonstrated a strong aromatic ring water accessibility dependence of the Tyr and Trp Raman cross sections, due to the dependence of their absorption wavelength maxima, and the concomitant dependence of their Raman excitation profiles to solvent exposure. We derived relationships that utilized solvatochromic environmental parameters to relate the aromatic ring environment to the Raman cross sections (*30*). The dependence of the Raman cross sections to water exposure was approximately linear over a significant range of water exposures. Thus, we can utilize a linear relationship between the Raman cross sections and the solvent exposure to estimate the changes in the Trp water exposure upon the acid unfolding of holoMb and apoMb:

$$A = (\sigma^\circ - \sigma_P)/m \quad (1)$$

where A is the total water-accessible surface area in square angstroms for the two Trp, σ_P is the total Trp Raman cross section of the two Trp in barns per molecule per sr, σ° is the total Trp Raman cross sections of the two fully buried Trp in Mb, and m is the slope of the dependence.

Table 2: Measured and Calculated Sum of the Raman Cross Sections and the Sum of the Solvent-Accessible Surface Areas for the Two Trp Residues of HoloMb and ApoMb[a]

	σ^{m}_{sum}	σ^{c}_{W7}	σ^{c}_{W14}	A_{W7}	A_{W14}	A_{sum}
holoMb at pH 7	3.20	1.50	1.70	56	22	78
holoMb at pH 2	1.10	0.55	0.55	217	217	434
apoMb at pH 7	2.68	1.11	1.70	122	22	144
apoMb at pH 4	2.04	0.55	1.70	217	22	349
apoMb at pH 2	1.10	0.55	0.55	217	217	434

[a] σ^{m}_{sum} is the measured sum of Raman cross section of two Trp residues, σ^{c}_{W7} is the calculated Raman cross section of Trp 7, and σ^{c}_{W14} is the calculated Raman cross section of Trp 14, given in barns per molecule per sr. A_{W7}, A_{W14}, and A_{sum} are the solvent-accessible surface areas of Trp 7 and Trp 14 and the sum of their exposed surface areas, given in square angstroms.

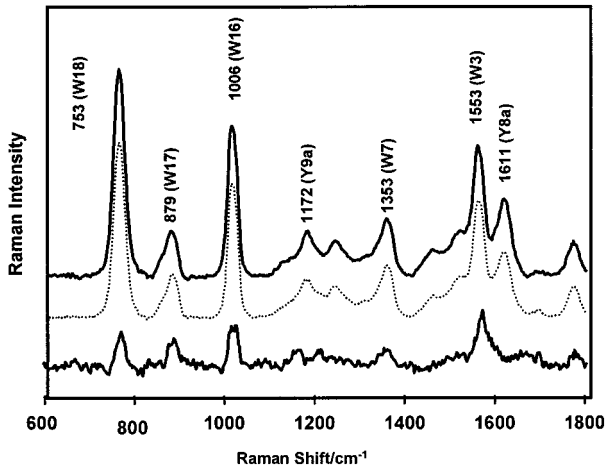

FIGURE 9: Raman spectra (229 nm excitation) of holoMb (—) and apoMb (•••) at pH 7.0 and the difference spectrum of holoMb minus apoMb (bottom). The concentrations of apoMb and holoMb are 80 μM.

We can calculate the parameters in eq 1 from the measured Raman cross sections of Trp in holoMb and of Trp monomer in water if we determine the water accessible surface areas in these two cases. A Trp monomer aromatic ring has a total surface area of of 217 Å^2 (*52*). In contrast, the horse holoMb X-ray structure indicates much smaller water solvent-accessible surface areas for Trp 7 and Trp 14 of 56 and 22 Å^2, respectively (*52, 53*). By using the measured sum of the Trp Raman cross sections of 3.20 b/(molecule·sr) in neutral pH holoMb (with a total surface area of 78 Å^2 for Trp 7 and Trp 14), and a Raman cross section of ~1.10 b/(molecule·sr) for the sum of the two fully water exposed Trp in unfolded holoMb at pH ~2.0 (*14, 52, 53*), we calculate $m = 0.0059$ b/(molecule·sr·Å^2) and $\sigma^{\circ} = 3.66$ b/(molecule·sr), respectively.

Thus, eq 1 can now be used to calculate the Trp water exposure in apoMb and holoMb at the different pH values. Table 2 lists the measured sum of the Raman cross sections and the sum of the solvent accessible surface areas for the two Trp residues of holoMb and apoMb. Table 2 shows that the 16% decreased Trp Raman cross sections [0.5 b/(molecule·sr)] in apoMb compared to holoMb neutral pH, as shown in Figure 9, is associated with a total increased water exposure of 85 Å^2. It is likely that this water exposure increase mainly occurs for Trp 7, which contacts the EF loop and helix H, instead of for Trp 14, which contacts residues in helices A, E, and G (*48*). This conclusion results from Eliezer and Wright's demonstration (*49*) that the EF loop and the F helix unfold upon removal of the heme in sperm whale apoMb, while the AGH helix domain remains intact in apoMb at neutral pH (*6*).

This conclusion is consistent with fluorescence studies of the individual Trp and a modified Trp 7 in native sperm whale apoMb, in which Postnikova et al. (*54*) found that the fluorescence maximum wavelength of Trp 14 (326 nm) is significantly shorter than that of Trp 7 (333 nm); longer wavelength emissions result from more solvent-exposed Trp residues, and a fully water-exposed Trp shows a λ_{max} of ~350 nm (*55, 56*).

The titration behavior of the total Trp cross sections in Figure 8 also suggest separate transitions for Trp 7 and Trp 14. The 0.7 b/(molecule·sr) cross section decrease associated with the apparent pK_a of 4 is calculated to be associated with a further 118 Å^2 increase in the Trp water exposure. It is likely that this increased water exposure mainly occurs for Trp 7 in view of the study of Postnikova et al. (*54*), which demonstrates little environmental change for Trp 14 until pH < 4 (*54*). Thus, the pH 4 apoMb intermediate would have Trp 7 essentially fully exposed to water, while Trp 14 is still well buried. Hughson et al. (*38*). measured amide deuterium exchange protection factor in sperm whale apoMb to determine intact tertiary and secondary structural domains in the pH 4 acid unfolding intermediate. They observed that the stable tertiary domain involving the A, G, and H helices shows significant protection factors for Trp 14.

The pH decrease from 4.0 to 2.0 results in a large decrease in the α-helical content and a 0.9 b/(molecule·sr) further decrease in the total Trp Raman cross section. The average Trp cross section becomes essentially identical to that of Trp monomer in water. Thus, this change in the Trp 14 Raman cross section must result from melting of helix A with an apparent pK_a of ~3, and the loss of its tertiary contacts with the G and H helix domain. Although it is possible that the acid titration of the Trp Raman cross section results from two structural transitions that expose both Trp residues together we believe this interpretation less likely: The magnitude of each change is just that required to fully water-expose an individual Trp and it does not seem likely that similar coupling exists for the two Trp to a single acid-induced structural change, especially for the higher pH titration where the A helix does not totally melt. Although we only have evidence for melting of the A helix around the two A-helix Trp residues, it is likely that the entire A helix is melted by pH 2 given the inherent instabilities of short α-helices.

Figure 8B shows that both apoMb and holoMb Tyr Raman cross sections remain constant as pH decreases. The invariance of the apoMb Tyr Raman intensities indicates that the Tyr environments do not change during acid denaturation; the G and H helices around the Tyr residues do not unfold. Thus, they remain intact at the lowest pH values used in this study.

Figure 10 shows the 229 nm excited Raman spectra of apoMb and holoMb at pH 2.0, and the featureless difference spectrum. Thus, the local environments of the Trp and Tyr in apoMb and holoMb at pH 2.0 are essentially identical. The existence of the heme has no impact on the protein structure at pH 2.0. From the pH dependence of the heme absorption spectra it is clear that the heme no longer resides

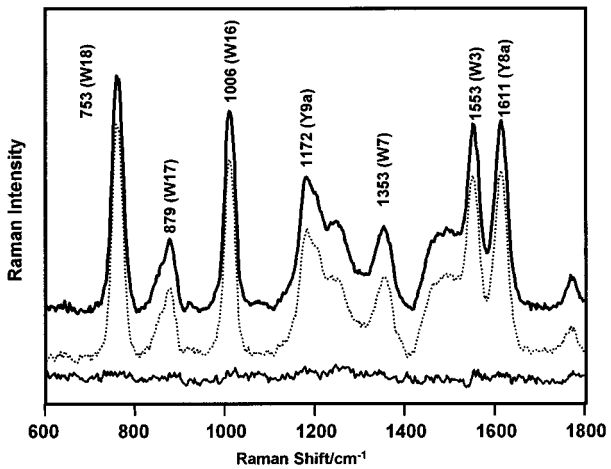

FIGURE 10: Raman spectra (229 nm excitation) of apoMb (—) and holoMb (•••) at pH 2.0 and the difference spectrum of apoMb minus holoMb (bottom). The concentrations of apoMb and holoMb are 80 μM.

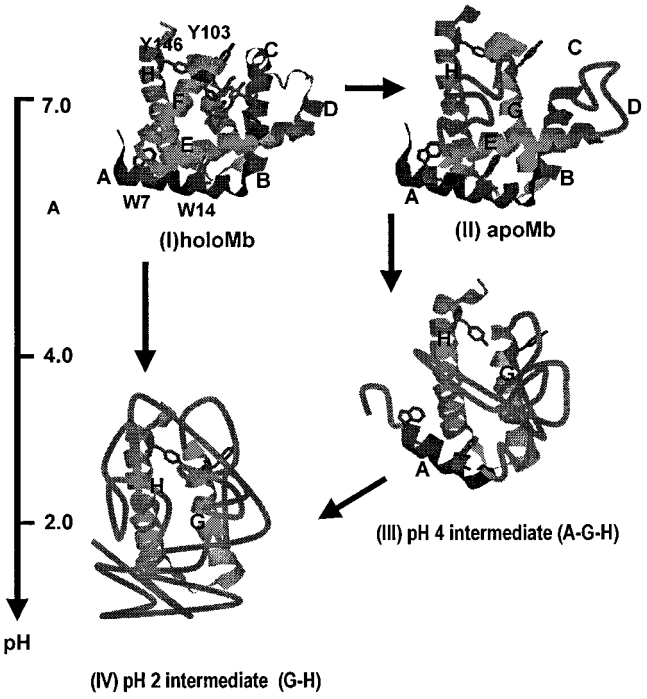

FIGURE 11: Structural model for acid denaturation of apoMb and holoMb. The helical structure is shown as ribbons and the unordered structure is shown as lines. The heme group, Trp 7, Trp 14, Tyr103, Tyr146, and His93 are shown. (I) Native holoMb; (II) native apoMb; (III) an apoMb pH 4 unfolding intermediate; (IV) an apoMb pH 2 unfolding intermediate. The solid arrows represent transitions due to pH decreases and the dashed arrow represents the removal of the heme group.

in the heme pocket but instead is probably weakly associated with the surface of the protein (*14*).

Figure 11 displays a structural model for the acid denaturation of apoMb and holoMb that involves (I) native holoMb, (II) native apoMb, (III) an apoMb pH 4 unfoldin-gintermediate, and (IV) an apoMb pH 2 unfolding intermediate. Conversion of pH 7 holoMb to pH 7 apoMb unravels the C, D, and F helices. The structural change results in alterations in the A helix or changes in A-helix tertiary contacts which partially expose Trp 7. A pH decrease to 4 has little impact on holoMb but forms a stable apoMb intermediate where the B and E helices are unfolded but a stable domain is preserved involving the A, G, and H helices. The Trp 7 residue becomes completely exposed to water while the Trp 14 residue remains mostly buried. Both holoMb and apoMb show further unfolding with an apparent pK_a ~ 3.5 to a state where most of the G and H helices remain, while all other helices are unraveled and where both Trp are fully exposed to water.

This model agrees with previous conclusions for structural alterations during the acid denaturation of Mb. Previously, Eliezer and Wright (*49*) proposed that the part of G and H helices near the amino terminus of the G helix in sperm whale apoMb are in fluctuating conformational states but are not unordered, while the NMR measurements of Hughson et al. (*6*) showed that the amino terminus of the G helix in native sperm whale apoMb is weakly protected from deuteration by the protein helical structure and that the amino terminus of the G helix remains folded. Eliezer and Wright (*49*) also conclude that the EF loop and F helix melt in horse apoMb. Our assignment of a fully intact AGH subdomain may somewhat conflict with Sabelko et al. (*11b*) who use the α-helical content calculated by CD to argue for some unfolding of the A helix. Our conclusion that the G and H helix remain at lowest pH is consistent with results of Hughson et al. (*6*) that the amino terminus of the G helix remains folded. Our conclusion also agrees with that of Rischel et al. (*57*), whose time-resolved Trp fluorescence study of horse apoMb concluded that in native horse apoMb and in the pH 4 apoMb folding intermediate, the A, G, and H helices remain.

We, however, cannot rule out the possibility of some G and H helix unraveling away from the Tyr with the simultaneous existence of some α-helical structure in the remainder of the protein.

CONCLUSIONS

We demonstrate here a powerful methodology that involves the simultaneous use of 206.5 nm excited Raman spectra to monitor changes of protein secondary structure and 229 nm excited Raman spectra to probe environmental changes and solvent exposures of Trp and Tyr side chains. We determined that native apoMb has ~62% α-helical structure and that removal of heme group in apoMb results in melting of the C, D, and F helices. Removal of the heme decreases the protein stability and causes apoMb to unfold at a higher pH value than holoMb. We conclude that neither holoMb nor apoMb fully unfolds even down to pH 1.5, where the G and H helix domains remain intact. For apoMb we observe the pH 4 intermediate, which involves linked helix A, G, and H domains. We see evidence for increased water exposure of Trp 7 in this pH ~4.0 intermediate.

These UV Raman measurements of protein structure have significant advantages over the conventional CD measurements, since side chains do not interfere with the secondary structure measurements. The Tyr and Trp solvent exposure measurements are immune from the confounding energy transfer and quenching interferences encountered by fluorescence. However, the greatest advantage of UV resonance Raman measurements is that they can be used kinetically in the picosecond, nanosecond, and microsecond time regimes to examine protein folding dynamics (*29*).

ACKNOWLEDGMENT

We gratefully acknowledge Mary Boyden for help in this work.

REFERENCES

1. Anfinsen, C. (1973) *Science 181*, 223.
2. Privalov, P. L. (1979) *Adv. Protein Chem. 33*, 167.
3. Privalov, P. L. (1982) *Adv. Protein Chem. 35*, 1.
4. Kim, P. S., and Baldwin, R. L. (1982) *Annu. Rev. Biochem. 51*, 459.
5. Kim, P. S., and Baldwin, R. L. (1990) *Annu. Rev. Biochem. 59*, 631.
6. Hughson, F. M., Wright, P. E., and Baldwin, R. L. (1990) *Science 249*, 1544.
7. (a) Jennings, P. A., and Wright, P. E. (1993) *Science 262*, 892. (b) Eliezer, D., Yao, J., Dyson, H. J., and Wright, P. E. (1998) *Nat. Struct. Biol. 5*, 148.
8. Fischer, D., Rice, D., Bowte, J. U., and Eisenberg, D. (1995) *FASEB J. 10*, 126.
9. Thornton, J. M., Jones, D. T., MacArthur, M. W., Orengo, C. M., and Swindells, M. B. (1995) *Philos. Trans. R. Soc. London B 348*, 71.
10. Hagen, S. J., Hofrichter, J., Szabo, A., and Eaton, W. A. (1990) *Proc. Natl. Acad. Sci. U.S.A. 93*, 11615.
11. (a) Ballew, R. M., Sabelko, J., and Gruebele, M. (1996) *Proc. Natl. Acad. Sci. U.S.A. 93*, 5759. (b) Sabelko, J., Erwin, J., and Gruebele, M. (1998) *J. Phys. Chem. 102*, 1806.
12. (a) Dill, K. A., and Chan, H. S. (1997) *Nat. Struct. Biol. 4*, 10. (b) Chan, H. S., and Dill, K. A. (1990) *Proc. Natl. Acad. Sci. U.S.A. 87*, 6388.
13. Takahashi, S., Yeh, S.-R., Das, T. K., Chan, C.-K., Gottfried D. S., and Rousseau, D. L. (1997) *Nat. Struct. Biol. 4*, 44.
14. Chi, Z., and Asher, S. A. (1998) *Biochemistry 37*, 2865.
15. Perutz, M. F., Kendrew, J. C., and Watson, H. C. (1965) *J. Mol. Biol. 13*, 669.
16. Teale, F. W. J. (1959) *Biochim. Biophys. Acta. 35*, 543.
17. Lecomte, J. T. L., Kai, Y.-H., and Cocco, M. J. (1996) *Proteins: Struct., Funct., Genet. 25*, 267.
18. Cocco, M. J., and Lecomte, J. T. L. (1990) *Biochemistry 29*, 11067.
19. Cocco, M. J., and Lecomte, J. T. L. (1994) *Protein Sci. 3*, 267.
20. Cocco, M. J., Kao, Y.-H., Phillips, A. T., and Lecomte, J. T. L. (1992), *Biochemistry 31*, 6481.
21. Johnson, C. R., Ludwig, M. L., O'Donnell, S., and Asher, S. A. (1984) *J. Am. Chem. Soc. 106*, 5008.
22. Song, S., and Asher, S. A. (1989) *J. Am. Chem. Soc. 111*, 4295.
23. (a) Asher, S. A. (1993) *Anal. Chem. 65*, 59A. (b) Asher, S. A. (1993) *Anal. Chem. 65*, 201A.
24. Cho, N., Song, S., and Asher, S. A. (1994) *Biochemistry 33*, 5932.
25. Chen, X. G., Asher, S. A., Scheitzer-Stenner, R., Mirkin, N. G., and Krimm, S. (1995) *J. Am. Chem. Soc. 117*, 2884.
26. Chen, X. G., Scheitzer-Stenner, R., Asher, S. A., Mirkin, N. G., and Krimm, S. (1995) *J. Phys. Chem. 99*, 3074.
27. Chi, Z., Chen, X. G., Holtz, J. S. W., and Asher, S. A. (1998) *Biochemistry 37*, 2855.
28. Cho, N., and Asher, S. A. (1995) *Biospectroscopy 2*, 71.
29. Lednev, I. K., Karnoup, A. S., Sparrow, M. C., and Asher, S. A. (1999) *J. Am. Chem. Soc. 121*, 4076.
30. Chi, Z., and Asher, S. A. (1999) *J. Phys. Chem B. 102*, 9595.
31. Longworth, J. W. (1971) *Excited States of Proteins and Nucleic Acids* (Steiner, R. F., and Weinryb, I., Eds.) p 432, Plenum Press, New York.
32. Edelhoch, E. (1967) *Biochemistry 6*, 1948.
33. Dudik, J. M., Johnson, C. R., and Asher, S. A. (1985) *J. Chem. Phys. 82*, 1732.
34. Walrafen, G. E. (1972) in *Water, A Comprehensive Treatise* (Frank, F., Ed.) Vol. 1, Chapter 5, Plenum Press, New York.
35. Asher, S. A., Johnson, C. R., and Murtaugh, J. (1983) *Rev. Sci. Instrum. 54*, 1657.
36. Holtz, J. S. W., Bormett, R. W., Chi, Z., Cho, N., Chen, X. G., Pajcini, V., Asher, S. A., Arrogoni, M., Owen, P., and Spinelli, L. (1996) *Appl. Spectrosc. 50*, 1459.
37. Asher, S. A., Bormett, R. W., Chen, X. G., Lemmon, D. H., Cho, N., Peterson, P., Arrigoni, M., Spinelli, M., and Cannon, J. (1993) *Appl. Spectrosc. 47,* 628.
38. Hughson, F. M., Barrick, D., and Baldwin, R. L. (1991) *Biochemistry 30*, 4113.
39. Rosenheck, K., and Doty, P. (1961) *Proc. Natl. Acad. Sci. U.S.A. 47*, 1775.
40. Asher, S. A., Chi, Z., and Li, P. (1998) *J. Raman Spectrosc. 29*, 927−931.
41. Sweeney, J. A., and Asher, S. A. (1990) *J. Phys. Chem. 94*, 4784.
42. Ludwig, M., and Asher, S. A. (1988) *J. Am. Chem. Soc. 110*, 1005.
43. Rava, R. P., and Spiro, T. G. (1985) *J. Phys. Chem. 89*, 1856.
44. Rava, R. P., and Spiro, T. G. (1984) *J. Am. Chem. Soc. 106*, 4062.
45. Nishii, I., Kataoka, M., and Goto, Y. (1995) *J. Mol. Biol. 250,* 223−238.
46. Goto, Y., Takahashi, N., and Fink, A. L. (1990) *Biochemistry 29*, 3480−3488.
47. Griko, Y. V., Privalov, P. L., Venyaminov, S. Y., and Kutyshenko, V. P. (1988) *J. Mol. Biol. 202*, 127−138.
48. Evans, S. V., and Brayer, G. D. (1988) *J. Biol. Chem. 263*, 4263.
49. Eliezer, D., and Wright, P. E. (1996) *J. Mol. Biol. 263*, 531.
50. Fotana, A., Zambonin, M., de Laureto, P. P., De Filippis, V., Clementi, A. and Scaramella, E. (1997) *J. Mol. Biol. 266*, 223.
51. Hughson, F. M., and Baldwin, R. L. (1989) *Biochemistry 28*, 4415.
52. Miller, S., Janin, J., Lesk, A. M., and Chothia, C. (1987) *J. Mol. Biol. 196*, 641.
53. Lee, B., and Richards, F. M. (1971) *J. Mol. Biol. 55*, 379.
54. Postnikova, G. B., Komarov, Y. E., and Yumakova, E. M. (1991) *Eur. J. Biochem. 198*, 223.
55. Eftink, M. R. (1991) *Methods Biochem. Anal. 35*, 127.
56. Lakowicz, J. (1983) *Principles of Fluorescence Spectroscopy*, Plenum, New York.
57. Rischel, C., Thyberg, P., Rigler, R., and Poulsen, F. M. (1997) *J. Mol. Biol. 257*, 877.

BI982654E